Full-Particle Simulation on Beam Electron Plasma in Linear Confinement System*)

Takaya MATSUI, Daigo ADACHI, Shuya IWATA, Takahiro URANO and Toshiki TAKAHASHI

Graduate School of Science and Technology, Gunma University, Gunma 376-8515, Japan

(Received 27 December 2017 / Accepted 27 March 2018)

Three-dimensional full particle simulation is performed on the electron beam plasma electrostatically confined in a linear chamber. Sausage instability and kink instability occurred within 1 μs from the initial state, and a twisted structure is also observed. The density distribution flattened with time and resultantly diffused in the radial direction. However, large scale collapse phenomenon until the beam plasma disappeared is not observed.

Keywords: electron beam plasma, full-particle simulation, sausage instability, kink instability, two-stream instability

DOI: 10.1585/pfr.13.3401041

1. Introduction

The concept of a compact neutron source by linear electrostatic confinement of deuterium ion beam was proposed by Momota *et al.* [1]. It is an attempt to use these for the cancer therapy [2, 3], for example, by confining an opposing beam of 30 keV in the reaction chamber and decelerating the 3.5 MeV neutron generated by the D-D reaction to give thermal or epithermal neutrons. Although this concept requires linear beam plasma confinement, there are concerns about the occurrence of many types of instability macroscopically such as kink and sausage instabilities and microscopically two-fluid instability. Securing simulation tools capable of reproducing these instabilities is entering an important phase. In this study, we aim to clarify the macroscopic behavior by carrying out a full particle simulation for linear beam plasma. In this study, we simulated electron beam plasma rather than ion beam for the purpose of capturing phenomena in a limited calculation time. Nonetheless, the relative speed of ions and electrons sets the same situation as the ion beam plasma that should be the target.

Proposals and simulation studies on neutron sources using z-pinch, for example, have been reported so far [4]. It has been found that the ion temperature must be higher than the electron temperature by a one-dimensional two-temperature MHD simulation model of the z-pinch that puffs TiD_2. However, a computational study based on a three-dimensional full-particle model that can handle the three-dimensional effect of macroscopic instability and field-particle interaction is not done in linear beam plasma.

author's e-mail: t-tak@gunma-u.ac.jp

*) This article is based on the presentation at the 26th International Toki Conference (ITC26).

2. Simulation Model

This section outlines the full particle simulation. We first describe the system of equations and then describe the setting of the simulation.

2.1 Full-particle simulation equations

In a full-particle model, we solve the equation of motion for ions and electrons

$$\frac{\mathrm{d}\mathbf{v}}{\mathrm{d}t} = \frac{q}{m}(\mathbf{E} + \mathbf{v} \times \mathbf{B}), \tag{1}$$

where $\mathbf{v}$ is the ions or electrons velocity, t is the time, $\mathbf{E}$ is the electric field, $\mathbf{B}$ is the magnetic field, and q and m are the charge and mass of the ions or electrons. We use the 4-th order Runge-Kutta method for time differentiation. The values of the electric and magnetic fields at the particle position in the calculation cell are obtained by linear interpolation from the values on the grid points constituting the cell.

The mass ratio of electrons and ions ($= m_\mathrm{i}/m_\mathrm{e}$) is not treated as a parameter, and they are adopted as actual values. The 30-keV electrons calculated in this study (whose speed is V) will have a Lorentz factor $1/\sqrt{1-(V^2/c^2)^2}$ of 1.06 and will be affected by the relativity somewhat. However, in conventional particle simulation, there are many researches that artificially reduce the mass ratio of ions and electrons for the purpose of reproducing longer time results among limited calculation resources. The results of this study show that the effect of mass increase due to relativistic effect is much less than that of artificial mass ratio. Although the classical equation of motion is adopted here, since the calculation cost does not change almost, a relativistic model will be used in the future.

The following Eqs. (2) - (5) are used for electromagnetic field calculation. We solve the wave equations for the scalar potential (2) and for the vector potential (3). The set

of equations is as follows:

$$\nabla^2\phi - \frac{1}{c^2}\frac{\partial^2\phi}{\partial t^2} = -\frac{\rho}{\varepsilon_0}, \tag{2}$$

$$\nabla^2\mathbf{A} - \frac{1}{c^2}\frac{\partial^2\mathbf{A}}{\partial t^2} = -\frac{\mathbf{j}}{c^2\varepsilon_0}, \tag{3}$$

$$\mathbf{j} = q_i n_i \mathbf{u}_i + q_e n_e \mathbf{u}_e, \tag{4}$$

$$\rho = q_i n_i + q_e n_e, \tag{5}$$

$$\mathbf{E} = -\nabla\phi - \frac{\partial\mathbf{A}}{\partial t}, \tag{6}$$

$$\mathbf{B} = \nabla \times \mathbf{A}, \tag{7}$$

where ϕ is the scalar potential, $\mathbf{A}$ is the vector potential, $\mathbf{j}$ is the current density, ρ is the charge density, ε_0 and μ_0 are the vacuum permittivity and permeability, $\mathbf{u}_i$ and $\mathbf{u}_e$ are the ion and electron flow velocities, and n_i and n_e are the ion and electron densities. In this study, $\mathbf{u}_i$, $\mathbf{u}_e$, n_i and n_e are calculated using the particle orbit calculation result of ions and electrons by the PIC method. Here, a collisionless plasma approximation is adopted.

In this study, the finite difference method is used for the spatial differentiation of the wave equation, basically applying the fourth-order central difference (5-point formula). Equations (2) and (3) are second order time differential equations for the four scalar functions. Here, the first derivative of a scalar function is introduced as a new variable. For example, for a scalar potential ϕ, we introduce a new scalar function η as

$$\eta \equiv \frac{\partial\phi}{\partial t},$$

and Eqs. (2) and (3) can form the first order time differential equation for the eight scalar functions. These are subjected to time integration using the fourth-order accuracy Runge-Kutta method, and the time evolution of the electromagnetic field is reproduced.

2.2 Settings of simulation

The calculation area and the plasma parameters are shown in Table 1. Here, we employ a three-dimensional Cartesian coordinates, and the number of simulation grid points are $N_x \times N_y \times N_z = 65 \times 65 \times 129$. The initial velocity of ions is assumed to follow the Maxwellian distribution in all x, y and z directions. The energy of the half of electrons is 30 keV and the initial velocity is determined as

$$v_{z0} = \sqrt{\frac{2E_e}{m_e}}. \tag{8}$$

The initial velocity in the x and y directions are 0. It is assumed that the remaining half of the electrons is in a stationary state. Calculated particles are handled as super-particles, and the weight of one super-particle is 10^6 as shown in Table 1.

Figure 1 shows our conceptual diagram of simulation model for electrons and ions. Electrons and ions are arranged according to the normal distribution in a cylindrical shape with a radius of 0.15 [m], which is a standard deviation of distribution.

Table 1 Parameters of reaction chamber and particles.

Calculation region length in x	1.0	m
Calculation region length in y	1.0	m
Calculation region length in z	2.0	m
Ion temperature	50	eV
Beam radius	0.15	m
Beam energy	30	keV
Number of super-particles (electron)	2.0×10^6	-
Number of super-particles (ion)	2.0×10^6	-
Weight of super-particles	10^6	-

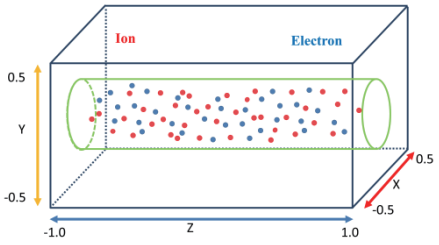

Fig. 1 Simulation model of electrons and ions.

The initial external magnetic field is zero and the initial scalar and vector potentials are calculated by solving the following Poisson's equations:

$$\nabla^2\phi = -\frac{\rho}{\varepsilon_0}, \tag{9}$$

$$\nabla^2\mathbf{A} = -\frac{\mathbf{j}}{c^2\varepsilon_0}. \tag{10}$$

In this research, periodic boundary condition is adopted in the axial direction for the purpose of preventing the inflow of various numerical noises from the boundary. Particles that reach the radial device boundary are treated as lost particles.

Also from Table 1, when the characteristic value of the density is $n_0 = 2.0 \times 10^{12}$ [m^{-3}], when evaluated by using this value, the electron plasma frequency ω_{pe} becomes 56.4 [GHz]. Therefore, the electron skin depth c/ω_{pe} is 5.31 [m], which is set to be larger than the grid size (~1.56 [cm]). In addition, the time step of the electromagnetic field is set to $c\Delta t$ =0.136 cm, and the time evolution of the electromagnetic field is numerically stable since the Courant condition is satisfied. If the ion temperature is equal to the electron temperature, the Debye length becomes 5.26 cm, which is about 3 times larger than the grid size. In the setting of this research, if super-particles are equally distributed in the calculation region, only 4 super-particles per cell are present. However, in the region where the beam is present, there are about 24 super-particles of both ion and electron on average. For this reason, the problem of statistical accuracy can be prevented by smoothing processing.

3. Results and Discussion

In this section, we will explain the results of the full particle simulation and discuss based on the results.

Figure 2 shows the temporal variation of the electron density distribution. Also, Fig. 3 shows the x-directional distribution of the electron density and the azimuthal direction component of the magnetic field at the same time. At 0.23 μs, coarseness appears in the z direction, which shows that it continues up to 0.45 μs. It can be seen that the density of the dense region with respect to the density of the coarse region is about a few times. After that, it can be seen that the density distribution has a meandering shape above and below the figure. Interpretation of this density distribution as a well-known instability suggests the occurrence of sausage instability, and the tortuous distribution suggests the occurrence of kink instability.

However, it is clear that each of these instabilities is saturated and it has not reached the point of collapsing the macroscopic structure. Since it is considered that the beam current and the resultant magnetic pressure are influenced by the instability growth, in the future it is necessary to execute a simulation for a larger current density case. In addition, it can be said from Fig. 2 that the peak value of the density distribution decreases with the lapse of time. The reason is that turbulence occurs in the electromagnetic field due to the occurrence of instability and electrons have radial velocity components.

According to the one-dimensional distribution diagram of Fig. 3, it can be seen that the density at the center increases to about $15n_0$ at 0.23 μsec. At this time, the magnetic field intensity in the azimuthal direction reaches about $-10B_0$, indicating that strong axial compression is being made. Here, the reference magnetic field B_0 is 0.126 [T]. This can be said to be just a typical example of sausage instability. However, it can be seen that asymmetry appears greatly during the next 0.45 to 0.68 μsec. Figure 4 shows three-dimensional visualization to express asymmetry in an easy-to-understand manner.

Figure 4 depicts an isosurface of a specified value for electron density. Here, we show a three-dimensional isosurface at the time when a characteristic shape appears as instability. The left end is the initial distribution. It is sausage instability that is observed at the earliest time of 0.19 μs. However, the columnar beam plasma continued to exist without breaking, and occurrence of kink instability at 0.31 μs is observed. Torsion of the beam plasma is observed at 0.50 μs due to the superposition of axial coarseness and kink instability.

There are two fluid instabilities as microscopic instability occurring in two particle groups with relative velocity. In order to observe this, we show the velocity distribution in Fig. 5. Here, 100,000 out of 2 million superparticles, one-twentieth thereof, are taken out and a histogram of the z component of velocity is drawn. Also, the horizontal axis is normalized by the initial beam velocity given by Eq. (8). For this reason, the initial distribution at the left end is present at $v_z/v_{z0} = 1.0$ and $v_z/v_{z0} = 0.0$ since half of the 50,000 electrons are present at $v_z/v_{z0} = 1.0$ and the other half are stationary. As time passes, changes in the macroscopic plasma shape and disturbance of the electromagnetic field occur, indicating that the speed spreads. In addition, some particles are accelerated by the electric field and it is also understood that the energy is increasing. However, no rapid change in the velocity distribution due to two-fluid instability was observed. One of the reasons is thought to be because the energy density of the plasma is small and the influence of the self-electric field and the self-magnetic field is small. Therefore, in order to further advance the study of the instability growth and the self-electromagnetic field, it is necessary to calculate the case

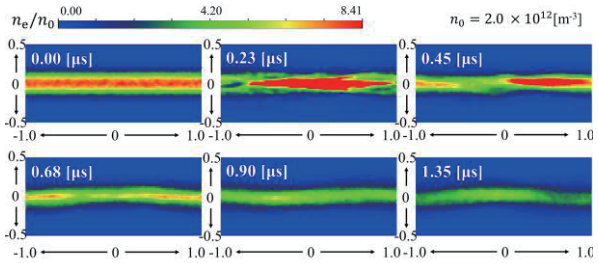

Fig. 2 Temporal change of electron density profile on the x-z plane.

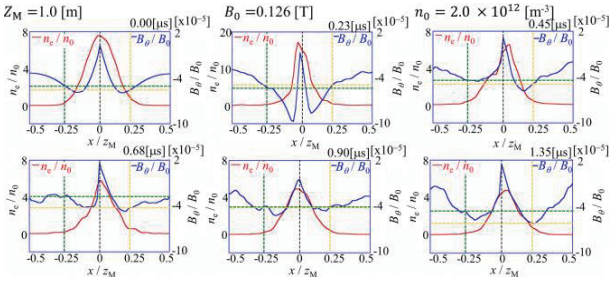

Fig. 3 Midplane profiles of electron density and θ component of magnetic field in the x direction.

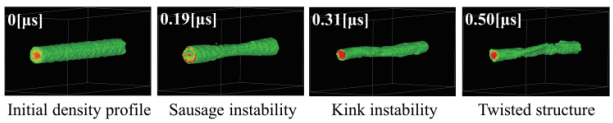

Fig. 4 Three-dimensional distribution of electron density.

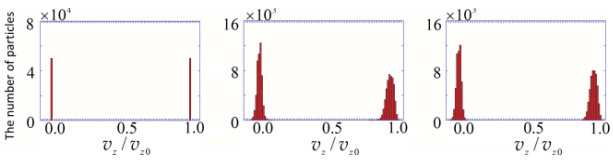

Fig. 5 Axial velocity distribution (0 [μs], 5.63 [μs], and 13.5 [μs]).

where the beam current is further increased by increasing the density by changing the weight of the super-particle.

4. Concluding Remarks

In this research, in order to clarify the three-dimensional effect of macroscopic instability and the interaction between the field and particles, a three-dimensional full particle simulation was performed on the electron beam plasma electrostatically confined in a linear chamber. Initially, cylindrical electron beam plasma was assumed. At the early stage of calculation, sausage instability and kink instability occurred, and the structure of twist was also observed. It was clarified that these instabilities cause disturbance in the electromagnetic field and promote flattening of the density radial distribution. However, large scale collapse phenomenon until the beam plasma disappeared was not observed. In addition, no microscopic instability appeared in velocity distribution function such as two-fluid instability was found. In order to investigate the growth of instability in detail, it is thought that calculation with higher energy density needs to be performed.

As an extension of this research, the research target is analysis of ion beam plasma by D-D beam. We believe that it is necessary to introduce the Monte Carlo collision operator such as Takizuka-Abe Model [5] and incorporate the interaction between ions and electrons.

Acknowledgements

This work is performed on "Plasma Simulator" (FUJITSU FX100) of NIFS with the support and under the auspices of the NIFS Collaboration Research program (NIFS17KNXN356 and NIFS15KNST087).

[1] H. Momota and G.H. Miley, J. Fusion Energy **28**, 191 (2009).
[2] C.A. Perks *et al.*, Br. J. Radiol. **61**, 1115 (1988).
[3] H. Tanaka *et al.*, Appl. Radiat. Isot. **69**, 1642 (2011).
[4] R.B. Baksht *et al.*, Phys. Plasmas **20**, 082701 (2013).
[5] T. Takizuka and H. Abe, J. Comp. Phys. **25**, 205 (1977).